AN IMPROVED DSP-BASED EIS INSTRUMENT USING REAL-TIME PERFORMANCE MONITORS AND PARAMETER ADJUSTMENT *

Greg M. Middlestead, Roger A. Green

ECE Department, North Dakota State University, Fargo, ND 58105-5285
E–mail: Greg.Middlestead@ndsu.edu, Roger.Green@ndsu.edu.

ABSTRACT

Electrochemical impedance spectroscopy (EIS) methods are commonly used to estimate the performance of corrosion resistant coatings. A multi-frequency EIS improves performance over traditional EIS systems through shortened trial times. With the addition of real-time performance monitors, a multi-frequency EIS system provides users with a better understanding of estimate quality and automatically adjusts a variety of parameters to further improve instrument performance. Such an automated multi-frequency EIS system is realized with modern digital signal processing (DSP) hardware.

1. INTRODUCTION

EIS instruments help assess the quality of corrosion-resistant coatings. Current commercial EIS systems do not adequately address extensive trial times, estimate quality, and nonlinear effects. We present techniques to improve EIS system performance by introducing a carefully designed perturbation signal and a method to monitor performance and adjust parameters. The improved signal and analysis techniques are developed for real-time DSP implementation.

1.1. EIS Basics

EIS systems apply a small perturbation signal to an electrochemical cell and measure the amplitude and phase of the resulting signal. A galvanostat applies a controlled current and measures the resulting voltage. A potentiostat applies a controlled voltage and measures the resulting current. Assuming the applied signal has a small amplitude, the cell can be approximated as a linear time-invariant (LTI) system. The i-th impedance estimate is found by $\hat{Z}_i(f) = \hat{V}_i(f)/\hat{I}_i(f)$, where $\hat{V}_i(f)$ and $\hat{I}_i(f)$ are from the i-th length-L DFTs of voltage and current, respectively.

Traditional EIS systems apply one frequency at a time over a typical frequency range of 10μHz to 300kHz [4]. Estimating the impedance at low frequencies is time consuming and introduces another concern: a typical cell's impedance is slowly time-varying. A quicker and potentially more accurate method is to estimate impedance using multiple frequencies at the same time, a technique known as multi-frequency EIS.

*SUPPORTED BY AFOSR/UDRI SUBCONTRACT RSC02050.

1.2. Prior Prototypes

NDSU researchers have developed several DSP-based multi-frequency EIS prototype systems. In all cases, the perturbation signal is a sum of sinusoids with a low peak-factor, which helps ensure high signal-to-noise ratio (SNR) operation within the linear region of the electrochemical cell.

The first prototype's perturbation signal is composed of linearly spaced frequencies [3]. A phase-optimization technique minimizes the peak-factor of the applied signal, and an FFT is used for DFT analysis.

Since a cell's impedance is typically plotted using a log-frequency scale, linear frequency spacing results in an overly large number of high-frequency terms while the low frequency range has sparse representation. A large number of terms reduces the per term SNR unnecessarily.

The second prototype exploits logarithmic frequency spacing to reduce the total number M of frequencies [5]. Rounding the frequencies toward nearby DFT bin frequencies f_k ensures signal periodicity, which is desirable given the DFT-based analysis. The reduced set of frequencies allows for increased SNR per term. Additionally, Goertzel processing ($\mathcal{O}(ML)$) is now comparable to the FFT ($\mathcal{O}(L \log_2 L)$). Goertzel's algorithm offers advantages over the FFT including low memory requirements (M versus L), reduced estimation latency due to recursive computation structures, and easy adjustment of DFT length L [7].

Elements from both prior prototypes are incorporated into the new system.

2. NEW CONTRIBUTIONS

The current prototype uses the same phase-optimization, similar pseudo-logarithmic frequency spacing, and Goertzel's algorithm to calculate the desired DFT coefficients. New contributions include automatic global gain adjustment, real-time performance monitors, and magnitude profile optimization. These new features increase the efficiency and accuracy over the earlier prototypes and provide more informative impedance spectra.

2.1. Global Gain Adjustment

The multi-frequency perturbation signal is applied to the cell. Signal gain is increased until significant nonlinear effects occur, as detected by monitoring harmonic frequency bins. By setting the signal gain just below this point, SNR is maximized for the target cell.

To appear in *12th IEEE DSP Workshop, Sept. 24-27, 2006, Jackson Lake Lodge, Wyoming*

2.2. Real-Time Performance Monitors

An estimate $\overline{Z}_n(f_k)$ of the true complex-valued impedance spectrum $Z(f_k)$ is formed by averaging the individual impedance estimates $\hat{Z}_i(f) = \hat{V}_i(f)/\hat{I}_i(f)$ over the available Goertzel blocks,

$$\overline{Z}_n(f_k) = \frac{1}{n}\sum_{i=1}^{n} \hat{Z}_i(f_k) \approx Z(f_k). \quad (1)$$

While there are many possible performance measures to establish and monitor the quality of $\overline{Z}_n(f_k)$, straightforward and effective choices are easily derived from the variance of $\overline{Z}_n(f_k)$, which is estimated as

$$\hat{\sigma}_n^2(f_k) = \frac{1}{n(n-1)}\sum_{i=1}^{n} |\hat{Z}_i(f_k) - \overline{Z}_n(f_k)|^2. \quad (2)$$

Estimator variance estimates provide the basis for statistical performance bounds.

Analogous to traditional confidence intervals, $|Z(f_k) - \overline{Z}_n(f_k)| < \alpha\hat{\sigma}_n(f_k)$ describes a confidence ball in the complex plane for $\overline{Z}_n(f_k)$, where α is selected to achieve the desired confidence level. Each ball, one for each frequency f_k, has a radius that is proportional to the corresponding standard deviation estimate $\hat{\sigma}_n(f_k)$. Each ball shrinks as the related impedance estimate converges toward its true value. By computing and monitoring the standard deviations $\hat{\sigma}_n(f_k)$, the performance of the estimated impedance spectrum at each frequency point is established.

To promote the efficiency required to realize real-time performance monitors, Eqs. (1) and (2) are replaced with their respective recursive forms [1]:

$$\overline{Z}_n(f_k) = \overline{Z}_{n-1}(f_k) + \frac{\hat{Z}_n(f_k) - \overline{Z}_{n-1}(f_k)}{n}, \quad (3)$$

and

$$\hat{\sigma}_n^2(f_k) = \left(\frac{n-2}{n}\right)\hat{\sigma}_{n-1}^2 + \frac{1}{n^2}|\hat{Z}_n(f_k) - \overline{Z}_{n-1}(f_k)|^2. \quad (4)$$

These forms are computationally efficient and suitable for real-time DSP system implementation.

A simple threshold applied to $\hat{\sigma}_n(f_k)$ provides an exit criteria for the EIS system. Once all standard deviations fall below the threshold, the quality of the estimated impedance spectrum is assured with a selectable level of confidence. This paper utilizes a fixed threshold across all frequencies f_k, which corresponds to an absolute, rather than relative, measure of quality; only simple modifications are required to accommodate relative, and other, measures of performance.

2.3. Magnitude Profile Optimization

Typical multi-frequency EIS systems utilize a flat magnitude spectrum for components of the perturbation signal. Although simple to construct, this approach has a significant flaw: since noise spectra are rarely flat in practice, a flat input spectrum causes the impedance estimates to converge at different rates. As a result, some estimates meet the exit criteria quite early while others take much longer. Simply turning these components off once the exit criteria is met is also unwise as the resulting transients adversely affect estimate quality. Thought of another way, power is wasted on components that meet the exit criteria early. The net result is a slower than necessary overall trial time. Given the very low frequencies typical of EIS systems, such delays can add many hours to a particular trial.

The estimated standard deviations $\hat{\sigma}_n(f_k)$ permit the magnitude profile to be set more optimally. Given the impedance estimates, the system adjusts the magnitude profile in an attempt to equalize the standard deviations $\hat{\sigma}_n(f_k)$ across the spectrum. One strategy is to simply scale the amplitude of each input frequency components by the corresponding standard deviation. When the standard deviations are approximately equal, the input spectrum is left unaltered, as desired. However, if the standard deviations are not equal, input components are strengthened or weakened as appropriate. Such a strategy ensures the exit criteria is met approximately at the same time for each frequency.

3. NEW PROTOTYPE AND RESULTS

The new DSP-based EIS prototype is built around a TMS320C6713 DSK, which is a high-end DSP development kit available from Texas Instruments (TI). A custom analog interface board (AIB) provides data conversion between the DSP and a custom-designed galvanostat board. For improved noise performance, the galvanostat and test cell are typically sealed in a Faraday cage. The galvanostat board is comprised of signal conditioning circuitry and the galvanostat. DSP-controlled signal conditioning attenuates the current to within the linear region of the cell and amplifies the voltage received from the galvanostat. The galvanostat is the circuitry needed to interface with the electrochemical cell, which is connected to the instrument using a reference electrode (RE), counter electrode (CE), and working electrode (WE). Figure 1 shows the EIS system block diagram.

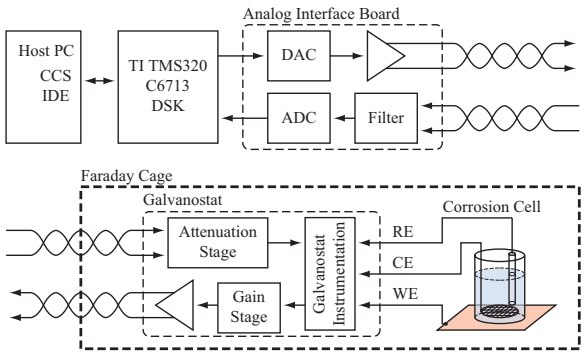

Fig. 1. EIS system block diagram.

To validate the theory and demonstrate the advantages of the developed multi-frequency EIS system, controlled simulations are performed in MATLAB. In these simulations, as well as later experimental trials, the periodic input is a pseudo-logarithmically spaced multi-tone perturbation signal with 25 component tones ranging from 1Hz to 100Hz. Using a sampling rate of 1kHz, the 6-second period of the input translates to an $L = 6000$ DFT length for each Goertzel block. The simulations employ a Randle's circuit, shown in

Fig. 2, which mimics the characteristics of an electrochemical cell. Roughly, R_S is the solution resistance, R_C is the cell resistance, and C_C is the cell capacitance. In this paper, these components are set to $R_S = 10\Omega$, $R_C = 10\text{M}\Omega$, and $C_C = 1\text{nF}$.

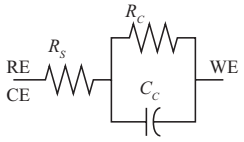

Fig. 2. Randle's circuit.

The known characteristics of the Randle's cell simplify algorithm verification. Colored noise, stronger at low frequencies than high, is then added to the output signal to simulate a real-life environment. To create the colored noise, Gaussian white noise is passed through a second-order Butterworth lowpass (LP) filter with 15Hz cutoff frequency.

Figure 3 shows the impedance magnitude spectra that result when an input with a flat magnitude spectrum is applied to the Randle's circuit. For this input, each tone is given an amplitude of 1. Following phase optimization, the peak amplitude of the input is 8.43, or about 34% of the worst case value of 25. The solid line shows the known theoretical magnitude spectrum $|Z(f_k)|$. Estimates $|\hat{Z}_i(f_k)|$ at block $n = 250$ demonstrate higher variability at low frequencies, as expected with the LP colored noise. Using all 250 Goertzel blocks, the magnitude of the average impedance estimate $|\overline{Z}_n(f_k)|$ displays convergence toward the true magnitude spectrum, again as expected, although some error is still visually discernable.

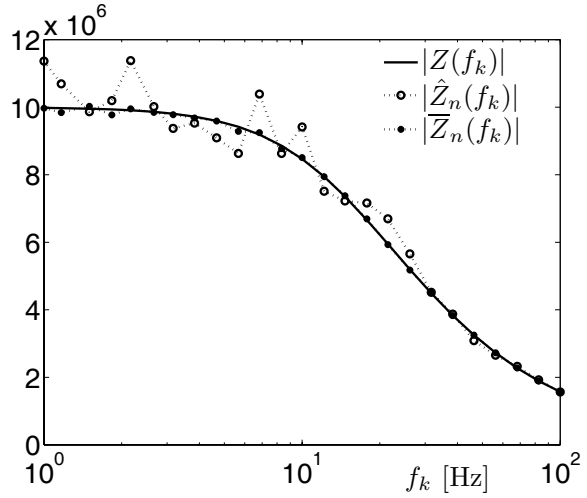

Fig. 3. Randle's circuit impedance magnitude spectra.

Figure 4 provides a better picture of estimator convergence as a function of block number n. Twenty five standard deviation $\hat{\sigma}_n(f_k)$ curves are shown, one for each of the 25 monitored frequencies f_k. Two features are notable from this plot. First, estimate quality improves with time, as shown by the general decay of each curve. Further, each of these decay rates are approximately equal. The second notable plot feature is that the curves corresponding to the high-frequency components are lower than the others; this is consistent with the LP colored noise which results in a higher SNR for the high-frequency terms. Using a threshold of 10^5, the dotted cross-hair shows that all estimates meet the exit criteria at block $n = 188$, which corresponds to a total trial duration of 18 minutes and 48 seconds.

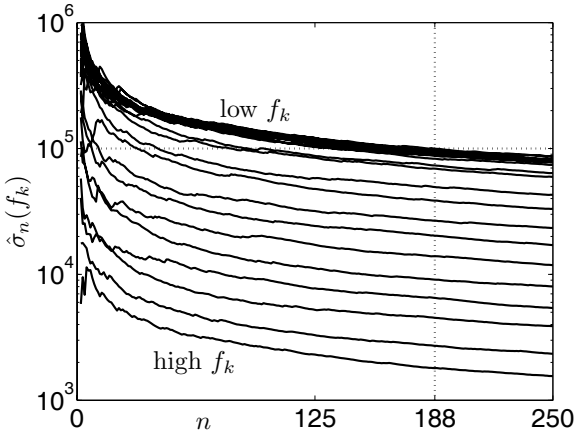

Fig. 4. $\hat{\sigma}_n(f_k)$ vs. n with flat input magnitude spectrum.

Figure 5 shows $\hat{\sigma}_n(f_k)$ vs. f_k for the values $n = 10$, 100, and 250. Again, two features are noteworthy in this plot. First, estimator quality improves with time, as evidenced by the drop in the level of the standard deviation curves with n. Second, estimator quality is not uniform across frequency, which again stems from the LP colored noise condition. Approximately half of the 25 input tones reside within the passband of the colored noise while the rest follow the 15Hz breakpoint. In fact, the $n = 250$ curve very closely follows the shape of the colored noise spectrum.

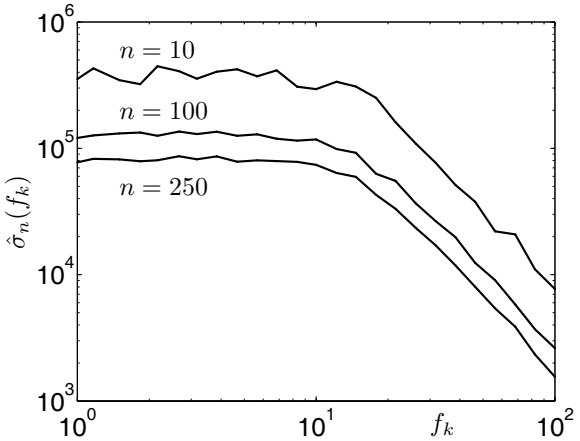

Fig. 5. $\hat{\sigma}_n(f_k)$ vs. f_k with flat input magnitude spectrum.

Looking at Figs. 4 and 5, it is clear that the impedance

estimates at the higher frequencies meet the exit criteria much earlier than the lower frequency terms. Input signal power is being wasted on these high-frequency components, which unnecessarily lengthens the overall trial duration. Thus, the input magnitude spectrum is adjusted to follow the shape of the $n = 250$ curve shown in Fig. 5, and the simulation is repeated. To allow fair comparisons, the power of this input is set equal to the power of the original input. Further, following phase optimization, the modified input has peak amplitude of 8.41, which is almost identical to the peak amplitude of the original flat spectrum input.

Figure 6 demonstrates the result of modifying the input signal's magnitude spectrum. Like Fig. 4, estimator quality improves with time. Unlike Fig. 4, however, the performance at any given frequency is approximately equal independent of f_k. This time, the exit criteria is met by all frequencies at $n = 81$, which corresponds to a total trial duration of 8 minutes and 6 seconds. This factor of 2.32 reduction in total trial time illustrates the value of properly adjusting the magnitude spectrum of the input perturbation signal. The amount of such improvements, of course, depends heavily on the nature of the underlying system noise; better and worse improvements in total trial times are possible.

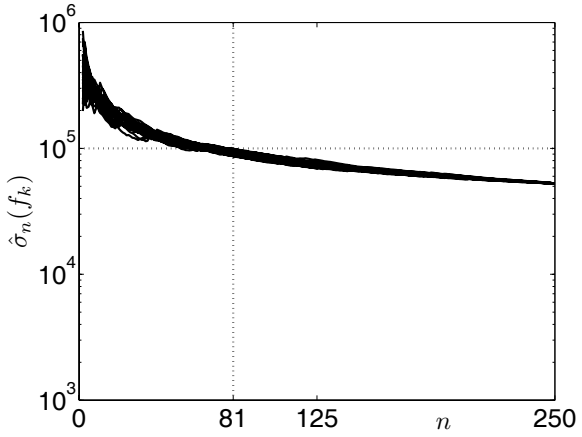

Fig. 6. $\hat{\sigma}_n(f_k)$ vs. n with modified input magnitude spectrum.

Similar to Fig. 5, Fig. 7 shows that estimator performance improves with time, as evidenced by the drop in the level of the standard deviation curves with n. More importantly, the figure also confirms that at any given time, estimator quality is approximately constant across frequency, which is the desired result of modifying the input magnitude spectrum.

Having demonstrated the potential benefit of the new system through simulation, the next step is to implement the techniques using DSP hardware and test the system using a physical load. Figure 8 shows the newly developed EIS prototype hardware, which follows the block diagram of Fig. 1. The AIB is mounted on the top of the 6713 DSK, both of which are located at the top of the figure, and the galvanostat board is located at the bottom of the photo. All algorithms are implemented in C and developed with the aid of TI's Code Composer Studio (CCS) integrated development

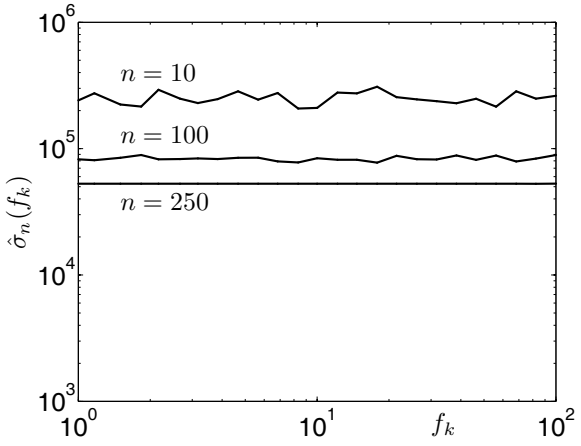

Fig. 7. $\hat{\sigma}_n(f_k)$ vs. f_k with modified input magnitude spectrum.

environment [2, 6, 8].

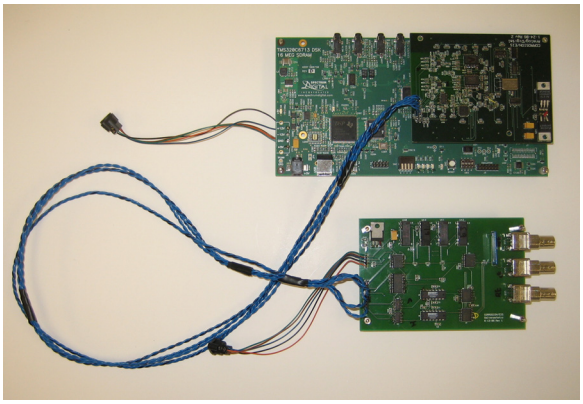

Fig. 8. EIS prototype.

Figure 9 shows the impedance magnitude spectrum that is measured by the EIS prototype when the input has a flat magnitude spectrum. A total of $n = 100$ blocks are measured, which corresponds to a trial time of about 10 minutes. The theoretical magnitude spectrum $|Z(f_k)|$ of the target Randle's circuit is derived from the measured component values of $R_S = 10.06\Omega$, $R_C = 10.25\text{M}\Omega$, and $C_C = 1.01\text{nF}$. Estimates $|\hat{Z}_i(f_k)|$ at block $n = 100$ as well as the average impedance estimate $|\overline{Z}_n(f_k)|$ are quite consistent, indicating low system noise. Overall, the measurements are reasonably close to the expected theoretical values; uncompensated system parasitics may offer some explanation for the differences between the estimates and theory.

Figure 10 plots the 25 standard deviation $\hat{\sigma}_n(f_k)$ curves as a function of processing block n. Several plot features are noteworthy. First, the relatively small standard deviations (small, at least, compared with Fig. 4 or 6) indicate relatively good initial measurement quality. Second, each curve displays the decay that is characteristic of improving estimate quality with time. The curves appear more noisy,

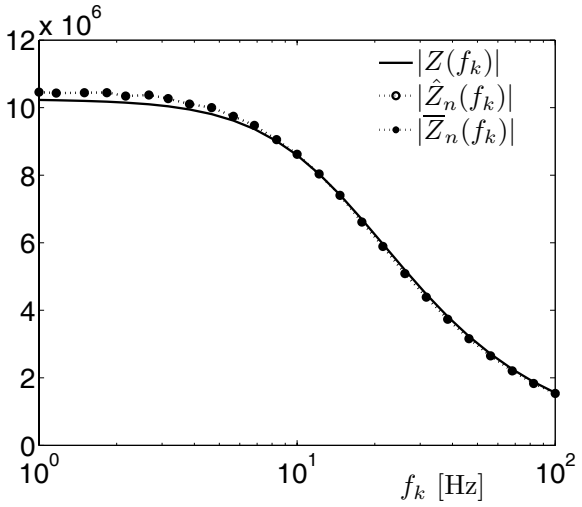

Fig. 9. Experimental Randle's $|Z(f_k)|$ and estimates.

and except for a single outlier, they all overlap. These traits suggest that a modified input magnitude spectrum will not offer much improvement in performance, something that is not too surprising given the low measurement noise and controlled testing environment. No satisfactory explanation of the $f = 11/6$Hz outlier curve has yet been determined. Additional work is required in this area as well as final system optimizations and tests on actual corrosion cells.

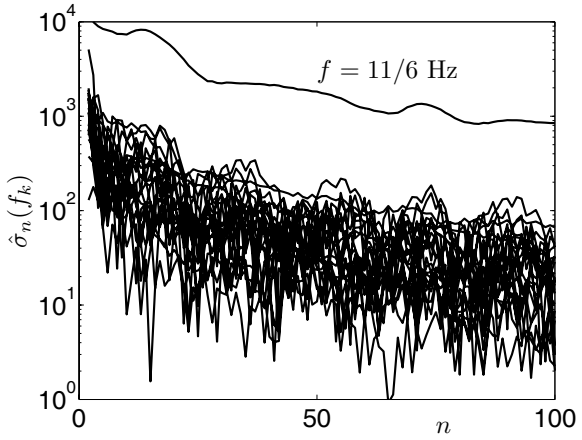

Fig. 10. Experimental $\hat{\sigma}_n(f_k)$ vs. n.

One of the most important results from the hardware trials does not appear in either Fig. 9 or 10. Independent of the measured data quality, the prototype tests verify that the algorithms can be successfully integrated into a real-time DSP-based EIS system.

4. CONCLUSIONS

New techniques for a DSP-based multi-frequency EIS system offer the potential to significantly reduce extensive trial times and provides more informative impedance spectra. This is achievable by creating algorithms that automatically adjust system parameters and monitor the performance of impedance estimates in real-time. Preliminary data collected from a DSP-based EIS prototype demonstrate algorithm feasibility, although additional work is necessary to optimize system performance and fully document algorithm effectiveness on actual corrosion cells under real-world conditions.

5. REFERENCES

[1] Casella, G., and Berger, R. L., *Statistical Interference,* Wadsworth, Inc., Belmont, California (1990).

[2] Chassaing, R., *Digital Signal Processing and Applications with the C6713 and C6416 DSK,* John Wiley & Sons, Inc., Hoboken, New Jersey (2005).

[3] Farden, D. C., Miramontes de León, G., and Tallman, D., "DSP-Based Instrumentation for Electrochemical Impedance Spectroscopy," Proceedings of the 195^{th} meeting of the Electrochemical Society, Vol. 99 No. 5, pp. 98-108, Seattle, WA (1999).

[4] "Electrochemical Impedance Spectroscopy Primer," Gamry Corporation Technical Report, available at http://www.gamry.com (2005).

[5] Green, R., Gelling, v., VonBank, H., and Harms, S., "DSP-based EIS Instrument Utilizing Low Peak-Factor Psuedo-Logarithmcally Spaced Multi-Frequency Test Signals," 207^{th} meeting of the Electrochemical Society, Quebec City, Canada (2005).

[6] Kelly, C. T., "Iterative Methods for Optimization," Society for Industrial and Applied Mathematics, Philadelphia (1999).

[7] Mitra, S. K., *Digital Signal Processing, A Computer-Based Approach,* 3rd Ed., McGraw-Hill, New York NY (2006).

[8] Welch, T. B., Wright, C. H., and Morrow, M. G., *Real-Time Digital Signal Processing from MATLAB® to C with TMS320C6x DSK,* CRC Press, Boca Raton, Florida (2006).